Available online at www.sciencedirect.com

SciVerse ScienceDirect

Scripta Materialia 66 (2012) 495–498

Scripta MATERIALIA

www.elsevier.com/locate/scriptamat

Electrochemical performance of template-synthesized CoSb nanowires array as an anode material for lithium ion batteries

You-wen Yang,[a,*] Fei Liu,[a] Tian-ying Li,[a] Yan-biao Chen,[a] Yu-cheng Wu[b] and Ming-guang Kong[c]

[a]*School of Chemical Engineering, Hefei University of Technology, Hefei 230009, People's Republic of China*
[b]*School of Material Science and Engineering, Hefei University of Technology, Hefei 230009, People's Republic of China*
[c]*Key Laboratory of Materials Physics, Institute of Solid State Physics, Chinese Academy of Sciences, Hefei 230031, People's Republic of China*

Received 22 November 2011; accepted 24 December 2011
Available online 2 January 2012

We etched the anodic alumina membranes around CoSb nanowires for different times and thereby obtained CoSb nanowire arrays with different degrees of order. Test results showed that highly ordered nanowire array structures have a charge–discharge capacity of more than 200 mA h g^{-1}, with a coulombic efficiency of 86% and a capability retention rate of 28% after 10 cycles. In this study, we provide evidence to support the hypothesis that a nanowire array structure is propitious in improving the performance of the anode material in lithium ion batteries.

Keywords: CoSb nanowires array; Li ion batteries; Electrodeposition; Anode material; Discharge capacity

The morphology and structure of the electrode materials used as anodes in lithium ion batteries (LIBs) materials significantly affect the electrochemical performance of the LIBs. The morphology and structure of one-dimensional (1-D) nanostructured electrode materials, such as nanowires (NWs), nanotubes (NTs) and nanofilms (NFs), have been widely investigated and adapted to achieve high-performance LIBs [1,2]. For instance, Chan et al. [3] used the vapor–liquid–solid method to fabricate Ge NW electrodes with an initial discharge capacity of 1142 mA h g^{-1} over 20 cycles at the 0.05C rate. Novel Si NT electrodes prepared by Park et al. [4] showed an ultrahigh reversible charge capacity of 3247 mA h g^{-1}, with a coulombic efficiency of 89% and superior capacity retention, even at a 5C rate. In addition, Villevieille et al. [5] synthesized NiSb NF electrodes by a solid-state reaction, which revealed an initial discharge of 446 mA h g^{-1} but displayed a rapid decline of reversible capacity. There is growing evidence that 1-D nanostructured electrode materials can improve the electrochemical properties of LIBs compared to their bulk counterparts [6]. Among these 1-D nanostructures, the NW has received much more attention due to its improvement of the rate capabilities of LIB anode materials [7]. The improved performance of NW is due to the following factors: (i) with each NW contacting the current collector, it possesses good electronic conduction along the length; (ii) it exhibits short Li insertion distances and a high interfacial contact area with the electrolyte; and (iii) it improves material durability owing to its nanostructure [8,9].

To develop alternative anode materials at low cost, extensive investigations have focused on exploring novel Sb-based intermetallic materials with high specific capacities [10–13]. In this respect, theoretical calculation has shown that an Sb-based alloy has a high specific capacity of 660 mA h g^{-1}, which is approximately twice that of graphitic carbon (372 mA h g^{-1}) [14]. In our previous paper, we reported the preparation of CoSb NW arrays fabricated by electrodeposition in anodic alumina membranes (AAM). The electrochemical performance of the CoSb/AAM NW arrays exhibited a high discharge capacity and charge capacity, but the AAM has a great influence on the performance of such NW arrays [15]. The challenge is how to dislodge the AAM and get highly ordered CoSb NW arrays, and then to further study their electrochemical properties. In this study,

* Corresponding author. Address: School of Chemical Engineering, Hefei University of Technology, No. 193 Tunxi Road, Hefei 230009, Anhui Province, People's Republic of China. Tel.: +86 551 2901165; e-mail: hfutyyw@163.com

1359-6462/$ - see front matter © 2011 Acta Materialia Inc. Published by Elsevier Ltd. All rights reserved.
doi:10.1016/j.scriptamat.2011.12.038

we focus on the charge–discharge characteristics of CoSb NWs array after etching the AAM for different times and attempt to demonstrate the merits of a highly ordered NW array structure.

The CoSb/AAM NW arrays were fabricated by pulsed electrodeposition [15]. The typical electrolyte for the electrodeposition consisted of 0.01 M $KSbOC_4H_4O_6{\cdot}1/2H_2O$, 0.2 M $CoCl_2{\cdot}6H_2O$ and 0.18 M H_3BO_3. The pH value of the electrolyte was adjusted to 3.5 and the fabrication was performed at 300 K at a voltage value of −2.6 V. Both the pulse times and the delay times were 500 μs. To get the CoSb NW anode array structure, we immersed the samples in 5 wt.% NaOH solution for different times to remove the alumina template and then washed them several times with deionized water.

The electrochemical performances were evaluated in two-electrode coin cells (CR2032). The working electrode was the CoSb NW array. A foil of pure lithium served as the counter electrode. A Celgard 2400 microporous polypropylene membrane was used as a separator. The electrolyte was 1 M $LiPF_6$ in a mixture of ethylene carbonate and dimethyl carbonate (1:1 in volume). The cells were assembled in a dry sealed glovebox filled with high-purity argon gas. The charge–discharge measurements were taken using a multi-channel battery test system (NEWARE BTS-610). The cells were galvanostatically discharged–charged in a voltage range from 0.05 to 4.5 V vs. Li^+/Li at a current density of 60 mAg^{-1} at ambient condition.

Figure 1 shows the charge (Li-deserting) and discharge (Li-inserting) curves of the CoSb/AAM NW array electrode without etching (a), and after etching for 2 min (b), 5 min (c) and 8 min (d), respectively. Comparing these four samples, one can see that the charge–discharge properties of the CoSb NW array electrode assembly change considerably with increasing etching time. It is clear that, aside from the first discharge process, these four synthesized CoSb NWs samples overall exhibit good reversibility, as indicated by the nearly overlapped charge and discharge curves.

As Figure 1(a) shows, the first discharge capacity of sample 1 is 1095 mA h g^{-1}. The main reduction reaction is in the first discharge process and occurs at a low plateau of 1.2 V, while in the subsequent discharge processes there are slope beginning at 0.6 V.

For sample 2 (Fig. 1(b)), the first discharge capacity of the CoSb NW array electrode etched for 2 min is 1061 mA h g^{-1}. This sample delivers a capacity of 245 mA h g^{-1} after 10 cycles.

For sample 3 (Fig. 1(c)), the first discharge capacity of the CoSb NW array electrode etched for 5 min is only 942 mA h g^{-1}, which is lower than both samples 1 and 2. However, this sample delivers a capacity of 267 mA h g^{-1} after 10 cycles, which indicates a more steady capacity. The well-defined plateau of the first discharge at about 0.25 V is due to the reaction of CoSb with Li^+ and the subsequent formation of Li_3Sb, while that of the subsequent discharge at nearly 0.6 V is due to the breakdown of CoSb structure, the reaction of Sb with Li^+ and the formation of Li_3Sb [16,17]. This means the CoSb structure is destroyed during the reaction of CoSb with Li^+. It can be seen from Figure 1(c) that the

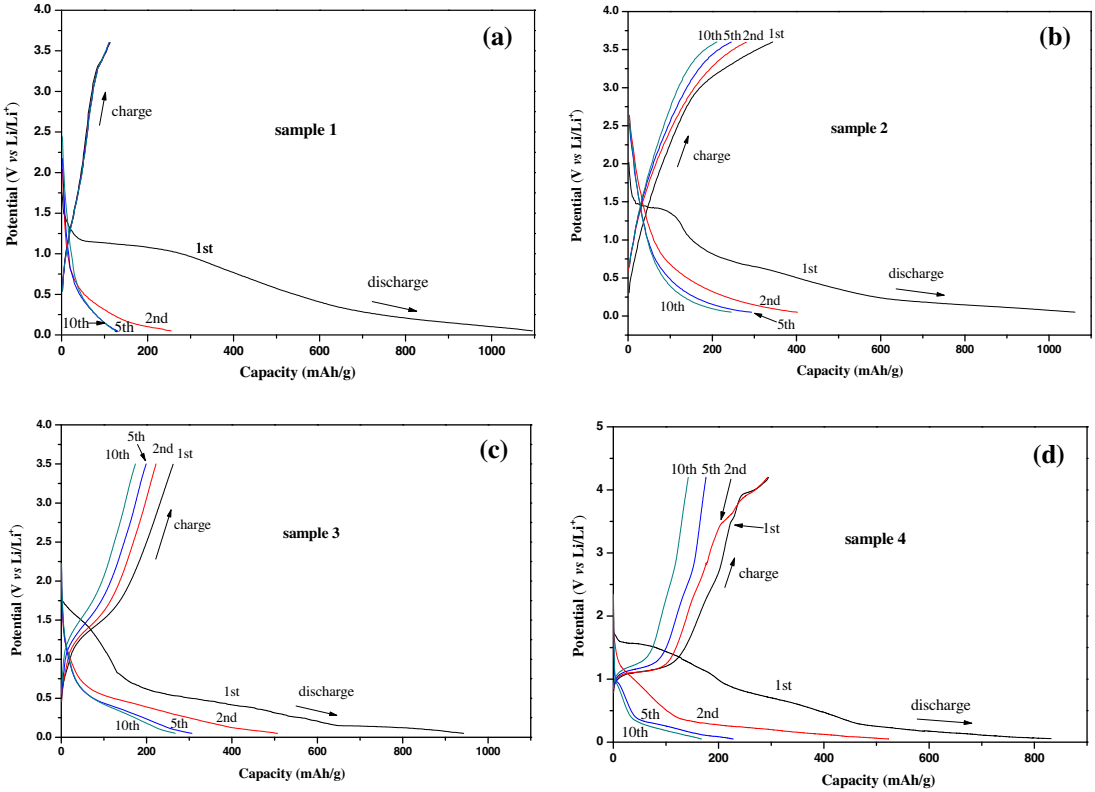

Figure 1. Charge–discharge curves of the CoSb NW array electrode without etching (a), and after etching for 2 min (b), 5 min (c) and 8 min (d), respectively.

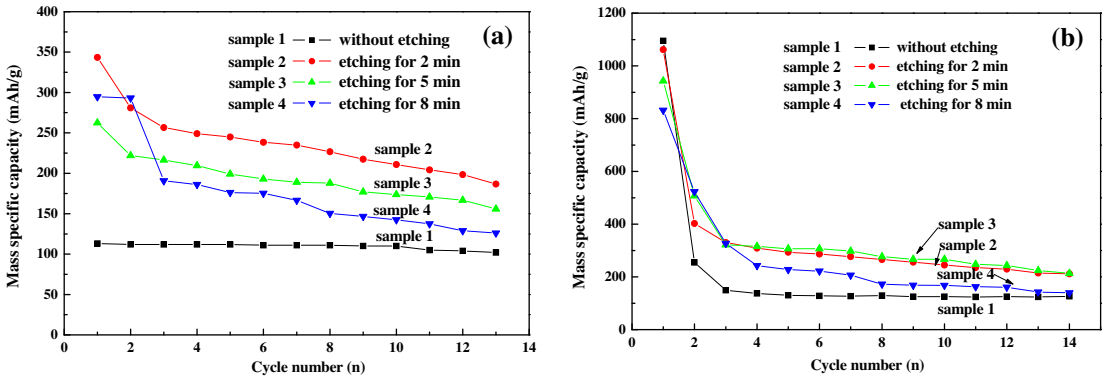

Figure 2. Charge (a) and discharge (b) cycle lives of samples 1–4, respectively.

subsequent charge and discharge cycles are reproducible with increasing cycle numbers, namely, the charge and discharge plateaus of CoSb NWs electrode are fixed at 1.25 and 0.6 V, respectively. This implies that reversible reactions occur after the first discharge. In addition, high anode working voltages will be of benefit to the safety of the charge and discharge processes by avoiding Li dendritic crystal growth.

As shown in Figure 1(d), the first discharge capacity of the sample 4 CoSb NW array electrode is 831 mA h g^{-1}, which is much lower than samples 1, 2 and 3. In addition, sample 4 delivers a capacity of less than 200 mA h g^{-1}, indicating a weaker electrochemical performance.

Figure 2 presents the charge (a) and discharge (b) cycle lives of samples 1–4. As expected, the electrochemical performance of the sample 1 is poor. This is attributed to the AAM. With increasing etching time, samples 2 and 3 have better charge–discharge capacities than sample 1. However, the charge–discharge capacity does not always increase with etching time: sample 4 clearly shows a rapid decrease in charge–discharge capacity as a function of cycle number. Furthermore, after 10 cycles, the discharge capacities of samples 2 and 3 are both maintained above 200 mA h g^{-1}, but the discharge capacity of sample 4 is about 160 mA h g^{-1}, which means that the Coulomb efficiency of sample 4 is poor. It can also be seen from Figure 2(b) that the capacity retention rate of sample 3 is above 28% after 10 cycles, and the discharge capability of the sample 3 is better than that of the sample 2.

Several factors that affect the electrochemical performance of the NW arrays as anode materials are as follows: the length and diameter of NWs; the structural integrity of the NW arrays; and contact with the current collector [18,19]. The length and diameter of NWs determine their surface area and the path length for Li ion transport. In a highly ordered NW structure, the open space between neighbouring NWs allows for easy diffusion of electrolyte into the inner region of the electrode. In our experiment, we fabricated the electrode by the pulsed electrodeposition method, and each NW is connected to the Au current collector. This is advantageous for the transport of charge and the irreversible reduction in capacity [20]. In this typical experiment, the CoSb/AAM arrays were etched with 5 wt.% NaOH solution for different times. As Figure 3(a) illustrates, before etching, the NW is totally encapsulated by AAM. In this case, Li^+ is transported only from the top of the wire, making it difficult for the Li^+ to become embedded and thus reducing the area of the NWs that is intercalated with Li. This also reduces the wettability of the CoSb NWs. More AAM is removed as the etching time increases (see Fig. 3(b) and (c)), thus exposing more of the CoSb NWs. This increases the wetting of the NWs and the diffusion of Li ions. Furthermore, increasing numbers of CoSb NWs participate in Li removal (insertion), thus improving the electrochemical performance of the CoSb NW arrays. However, the larger specific surface area can promote the decomposition of electrolytes and the formation of a solid electrolyte interphase

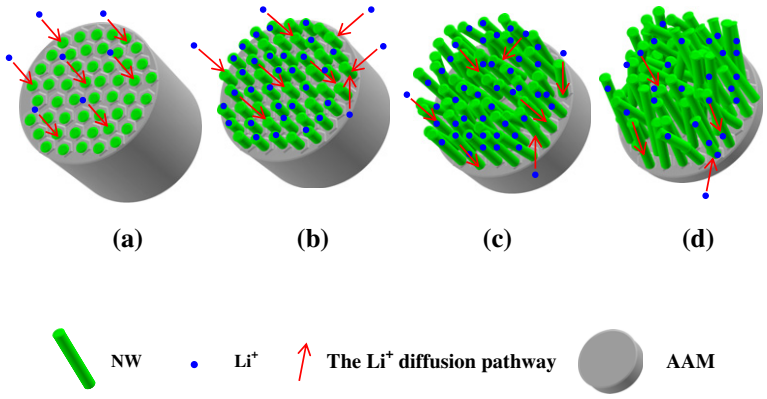

Figure 3. Schematic structure chart of CoSb NW arrays without etching (a), and after etching for 2 min (b), 5 min (c) and 8 min (d), respectively.

layer [21,22], resulting in the irreversible increases in capacity. However, the concrete cause needs to be studied further. As the etching time increases to 8 min or more (Fig. 3(d)), the bare NWs are no longer parallel. The agglomeration of NWs will lead to the deterioration in contact between the electrode and the electrolyte, and a longer transmission path for Li ions. At the same time, as the number of broken NWs increases, the contact between the NW arrays and the Au current collector will become poorer, causing the conductive efficiency to decrease. We can thus see that the electrochemical cycling performance of sample 4 degrades drastically.

In summary, on the basis of the successful synthesis of an array of CoSb NWs reported in our previous paper, we have further investigated their electrochemical performance when they act as an anode material for LIBs. By comparison, the electrochemical performance measurements show that the CoSb NW array electrode etched with 5 wt.% NaOH solution for 5 min displays better capacity retention and a higher discharge capacity. Moreover, the testing results show that the first irreversible capacity decreases continually with increasing etching time, and the highly ordered NW array structure improves the charge–discharge capacity and cycle life for LIBs. Optimization of the NW structure is therefore a promising way to improve the electrode materials for LIBs. We are constantly seeking to improve the electrode fabrication process to highlight the advantage of the NW array structure, and to further study the mechanism of lithium intercalation/deintercalation.

The project was supported by the Anhui Provincial Natural Science Foundation (11040606M52), the Science and Technology Planning Project of Anhui Province (10020203070) and the Major Research plan of the National Natural Science Foundation of China (91021030).

[1] Y. Yao, M.T. Mcdowell, I. Ryu, H. Wu, N. Liu, L.B. Hu, W.D. Nix, Y. Cui, Nano Lett. 11 (2011) 2949–2954.
[2] J. Hassoun, G.A. Elia, S. Panero, B. Scrosati, J. Power, Sources 196 (2011) 7767–7770.
[3] C.K. Chan, X.F. Zhang, Y. Cui, Nano Lett. 8 (2008) 307–309.
[4] M.H. Park, M.G. Kim, J. Joo, K. Kim, J. Kim, S. Ahn, Y. Cui, J. Cho, Nano Lett. 9 (2009) 3844–3847.
[5] C. Villevieille, C.M. Ionica-Bousqurt, A.D. Benedetti, F. Morato, J.F. Pierson, Solid State Ionics 192 (2011) 298–303.
[6] K.T. Nam, D.W. Kim, P.J. Yoo, C.Y. Chiang, N. Meethong, P.T. Hammond, Y.M. Chiangm, A.M. Belcher, Science 312 (2006) 885–888.
[7] J.H. Kim, T. Ayalasomayajula, V. Gona, D. Choi, J. Power, Sources 183 (2008) 366–369.
[8] X.L. Li, P.P. Li, M. Luo, X.Y. Chen, J.J. Chen, J. Solid State Electrochem. 14 (2010) 1325–1332.
[9] R. Huang, J. Zhu, Mater. Chem. Phys. 121 (2010) 519–522.
[10] G. Ferrara, L. Damen, C. Arbizzani, R. Inguanta, S. Piazza, C. Sunseri, M. Mastragostino, J. Power, Sources 196 (2011) 1469–1473.
[11] F. Wang, M.S. Zhao, X.P. Song, J. Alloys Compd. 472 (2009) 55–58.
[12] C.M. Park, H.J. Sohn, Electrochim. Acta 55 (2010) 4987–4994.
[13] M.W. Wang, H.L. Zhao, J.C. He, R.L. Wang, J.B. Chen, N. Chen, J. Alloys Compd. 484 (2009) 864–869.
[14] W.J. Zhang, J. Power Sources 196 (2011) 13–24.
[15] Y.W. Yang, Y.B. Chen, F. Liu, X.Y. Cheng, Y.C. Wu, Electrochim. Acta 56 (2011) 6420–6425.
[16] J. Xie, G.S. Cao, Y.D. Zhong, X.B. Zhao, J. Electroanal. Chem. 568 (2004) 323–327.
[17] V. Pralong, J.B. Leriche, B. Beaudoin, E. Naudin, M. Morcrette, J.M. Tarascon, Solid State Ionics 166 (2004) 295–305.
[18] Y.D. Ko, J.G. Kang, J.G. Park, S.J. Lee, D.W. Kim, Nanotechnology 20 (2009) 455701.
[19] K.S. Park, J.G. Kang, Y.J. Choi, S.J. Lee, D.W. Kim, J.G. Park, Energy Environ. Sci. 4 (2011) 1796–1801.
[20] Y.M. Li, X.J. Lv, J.H. Li, Appl. Phys. Lett. 95 (2009) 113102.
[21] J. Xie, X.B. Zhao, G.S. Cao, M.J. Zhao, S.F. Su, J. Power, Sources 140 (2005) 350–354.
[22] P.L. Taberba, S. Mitra, P. Poizot, P. Simon, J.M. Tarascon, Nat. Mater. 5 (2006) 567–573.